E-Journal of Advanced Maintenance Vol.5-2 (2013) 113-120
Japan Society of Maintenology

On the Efficiency of Direct Sparse Solver for FEM-ECT Analysis

Shigeru HEMMI [1,*], Masayuki SARUHASHI [1] and Yasushi IKEGAMI [1]

[1]*Itochu Techno-Solutions Corporation, Kasumigaseki Bldg, 3-2-5 Kasumigaseki, Chiyoda-ku, Tokyo 100-6080, Japan*

ABSTRACT

In the analysis of time harmonic eddy current testing (ECT) by FEM, in which non-cored exciter/detector coils are moved above the surface of metal object, the use of direct sparse solver has been studied. And it is found practically efficient because the factorized numerical matrix can be reused repeatedly in the calculation. The validity of this method is discussed and a satisfactory result for an ECT model is shown.

KEYWORDS

Eddy Current Testing, ECT, Finite Element Methods, FEM, Direct Sparse Solver, MUMPS, Edge Element, Coulomb Gauge

ARTICLE INFORMATION

Article history:
Received 9 November 2012
Accepted 10 June 2013

1. Introduction

In Finite Element Method (FEM) model for the analysis of Eddy Current Testing (ECT), especially for the case of time harmonic type, we have to treat sparse simultaneous equations composed by complex numbers, that bring about a larger scale calculation. To solve such equations efficiently, many authors tend to prefer iterative numerical solver, e.g., ICCG method[1,2,3,4]. However, in this paper, it is emphasized that direct sparse solver is also practically efficient, if the problem size is not very large, and the moving coils do not involve ferromagnetic core, because the factorized matrix for the first step in stepwise coil movement can be reused efficiently in the calculation routines of following steps.

2. Formulation and Direct Sparse Solver

2.1. Assumptions and Implementation Detail

In this note, only forward analysis is examined, not for inverse analysis. The phase convention of time harmonic factor $\exp(+j\omega t)$ is assumed where ω is angular frequency. Four vector potentials $(\mathbf{A},\varphi)$ are used as fundamental electromagnetic variables in SI units. The potential $\mathbf{A}$ is approximated by edge-based functions[5,6,7], whereas φ is approximated by nodal-based functions. Only the lowest order shape functions are applied for both edge variables and nodal variables. Since the electric displacement current is neglected, nodal φ within space meshes are not included; electric fields in space region are assumed to be dependent quantities of other variables. For the numerical samples herein, no boundary conditions applied except explicitly specified. Three types of FEM element libraries are implemented in our code, i.e., hexahedra, penta(prism) and tetra. Tetra elements are not used within this note because of its lower accuracy.

In our formulation, some aspects differ from other authors. Some differences excepting direct solver usage, are summarized as follows:

- Total vector potentials are adopted; some authors are using reduced vector potentials[2].
- Since the space or vacuum is a type of electromagnetic substances, the space involving both surrounding region and crack region are also meshed. Contrary to ours, crack region is not meshed by some authors[4].
- Since meshing exciter/detector coils together with space and conductor as an integrated FEM mesh is not an easy task, coil portions are not meshed as an integrated FEM mesh. Instead, equivalent electric currents are applied to FEM edges as a right hand side of linear simultaneous equations.
- The authors prefer Coulomb gauge fixing[8], i.e. $div\mathbf{A}=0$ (or rigorously $\varphi \neq 0 \,\&\, div\mathbf{A}=0$), rather

*Corresponding author, Tel: +81-3-6203-7450, E-mail: magna@ctc-g.co.jp

than $\varphi = 0$ gauge (or rigorously $\varphi = 0 \,\&\, div\mathbf{A} \neq 0$ gauge).
Although the $\varphi = 0$ gauge is not popular in conventional books of electromagnetism, samples of $\varphi = 0$ gauge are easily seen if the gauge transformation is applied to the problems in which Coulomb gauge solutions are available. For example, consider an electric capacitor problem of static voltage exerted. For this sample, $\varphi \neq 0$ and $\mathbf{A} = \mathbf{0}$ is obtained by solving, e.g., Laplace equation, with proper boundary conditions, and then if the gauge transformation is applied to this static problem so that it satisfies $\varphi = 0$, then $div\mathbf{A} \neq 0$ is obvious in it. The $\varphi = 0$ gauge is sometimes seen in other author's work of eddy current analysis, for example, see [2,9].

2.2. Ampere-Maxwell Equation in Weak Form and Singular Matrix of Edge Based Elements

The starting equation is Ampere-Maxwell equation expressed in term of four vector potentials $(\mathbf{A}, \varphi)$. Then standard procedure of FEM is applied, i.e. multiplication with some weight functions and integration over the entire domain. This is a weak form of Ampere-Maxwell equation.

$$\int_{\Omega} \mathbf{w} \cdot \left[rot\nu rot\mathbf{A} - \sigma\left(-j\omega\mathbf{A} - grad\varphi\right)\right] dV = \int_{\Omega} \mathbf{w} \cdot \mathbf{J}_{ExciteCoil} dV \qquad (1)$$

Here symbols ν, σ stand for magnetic reluctivity and electric conductivity respectively. The symbol $\mathbf{J}_{Excite\,Coil}$ is current density supplied to the exciter coils and dV is volume of the differential element and Ω is volumetric area of the entire domain involving both space and conductors.

For the weight function $\mathbf{w}$, the two weight functions are applied simultaneously. One is $\mathbf{w} \equiv \delta\mathbf{A}$ that satisfies $div(\delta\mathbf{A}) \cong 0$ and the other is $\mathbf{w} = grad(\delta\varphi)$ that satisfies $rot(grad(\delta\varphi)) \equiv 0$. The latter one corresponds to the conservation law of electric current.

For a hexahedral edge element of rigid rectangular shape, the divergence in the approximated field is zero, because the edge shape functions themselves may have a zero divergence [7]. However, if hexahedral shape is deformed and not rectangular shape, divergence free feature of fields may be an approximation. Then the weight function can be expected to satisfy $div(\delta\mathbf{A}) \cong 0$.

Approximate divergence free feature of the edge shape functions is a fundamental basis of divergence free nature of numerical solution of entire domain. However, it is not sufficient condition to get divergence free numerical solution. It is a well known fact that if gauge fixing is abandoned in edge element method, the matrix becomes singular one in the course of numerical process[4]. This causes a difficulty upon iterative and also direct solvers. Therefore, for this code using edge-based elements the diagonal components in assembled matrix are changed by adding very small values, in order to avoid the occurrence of singular matrix.

2.3. Right Hand Side of Simultaneous Equations

Since the total vector potentials are used instead of reduced potentials in the formulation, the calculation method for right hand side (r.h.s.) of equation (1) is necessary to be clarified. The exciter/detector coils are divided into "meshes" but these "meshes" are not directly used in the simultaneous equations of FEM. The r.h.s. of equation (1) is calculated through Biot-Savart integration so that FEM edges have proper and equivalent exciting currents.

Paying attention to exciter coils system, the following equation is an identity based on Biot-Savart law,

$$\mathbf{J}_{ExciteCoil} = rot\,\mathbf{H}_{ExciteCoil} = rot\left[\frac{1}{4\pi}\int_{\Omega} \frac{\mathbf{J}_{ExciteCoil} \times \mathbf{r}}{r^3} dV\right] \qquad (2)$$

where $\mathbf{J}_{ExciteCoil}$ is the prescribed current density on exciter coils and $\mathbf{H}_{ExciteCoil}$ is the corresponding magnetic field.

When a discrete mesh structure of the model is made, the above can be rewritten as follows to obtain an approximate value.

$$\mathbf{J}_{edge} = rot\left[\frac{1}{4\pi}\int_{\Omega}\frac{\mathbf{J}_{ExciteCoil}\times\mathbf{r}}{r^3}dV\right] \quad (3)$$

where $\mathbf{J}_{ExciteCoil}$ is defined only for exciter coil region. However, in the case of non-FEM meshes, any unknown variable are not assigned even where $\mathbf{J}_{ExciteCoil}$ resides. On the other hand, in case of $\mathbf{J}_{edge}$ it is defined on all edges of FEM-elements and unknown variables of simultaneous equations are assigned. The calculated column of $\mathbf{J}_{edge}$ from this equation (3) forms the r.h.s. of simultaneous linear equations of electromagnetic FEM based on total vector potentials.

2.4. Electromotive Force or Impedance of Detector Coil

The voltage or electromotive force induced along the detector coil wire, is described as

$$V_{e.m.f} = -j\omega\oint\mathbf{A}\cdot d\mathbf{l} \quad (4)$$

where $\mathbf{A}$ is the vector potential on the integration line and $d\mathbf{l}$ is the length of discrete element along the integration line of detector coil.

The vector potentials $\mathbf{A}$ in equation (4) are calculated as follows. For each FEM elements, the vector potentials at the element centers are obtained by the formula

$$\mathbf{A}_e = \sum_{i\in ElementEdges} A_i\mathbf{N}_i\big|_e \quad (5)$$

where the subscript e stands for element center, i runs over all edges of the specific element, A_i is the edge potential as the result of FEM computation, and $\mathbf{N}_i\big|_e$ is the value of vector shape function at the element center. The explicit form of vector shape function $\mathbf{N}_i$ is given in [7]. Calculating the vector potential value at an arbitrary point, i.e., a point on the line integration line, is a problem of interpolating scattered data. In our case, interpolation is completed using above scattered element center values by the formula:

$$\mathbf{A} = \sum_e w_e\mathbf{A}_e / \sum_e w_e \quad (6)$$

where e runs over all FEM element center and w_e are positive scalar weights for interpolation. In this code, $w_e = 1/r^4$ is chosen to enhance the contributions of closer elements much more, where r is the distance of element center and integration point. There is no deeper inspection of our choice of weight function; it was chosen because it is simple, robust and easy to code.

The change in induced voltage on detector coil is evaluated by the difference between values obtained for plates with crack and without crack.

2.5. Direct Sparse Solver

In numerical ECT analysis, problems often tend to be a larger size. One reason is that the crack size is so small that it requires finer mesh at the vicinity of cracks. The second reason is that exciter/detector coils are also small and move around the metal plate to search flaws. Consequently the mesh should be considerably fine for almost all regions involving metal plate and coil movement.

The use of sparse direct solver, in the context of three-dimensional FE modeling of Maxwell equations, has been limited due to the requirement for larger memory size and longer CPU time. Since CPU execution time of numerical factorization is proportional to DOF^3, practical limit of the efficiency of direct sparse solver is a severe obstacle. That is one of the reasons why most authors prefer iterative solvers [1,2,3,4,9]. Nevertheless, we choose direct solver here because of its

robustness for such intricate computation and growing capability of recent computer hardware making the direct solver applicable within a reasonable size. Within our limited hardware, 2 million complex DOF is close to the limit of our calculation at this moment.

As an efficient direct sparse solver, we chose an open source sparse direct solver, MUMPS [10]. MUMPS itself can work in MPI environment, which can be another measure expanding the model scale, but the function is not utilized here.

3. Code Validation

Some sample problems are described here to validate the code. The first one (*A.*) is the problem of an infinitely long and axially symmetric solenoid coil as a sample having rigorous theoretical solution. The second one (*B.*) is a comparison between perfect wire ring and ring with a cut, both of which are exerted by a low frequency magnetic field. This sample highlights a significance of the $-grad\varphi$ term in Coulomb gauge. And the last one (*C.*) is a benchmark on ECT, where an impedance profile is obtained as the result and compared with that of a published experiment.

A. Infinite Axially Symmetric Solenoid

Here an infinite solenoid coil problem is solved. The problem is a mimic of the sample in Adventure project [9]. As seen in Fig. 1, an infinite cylindrical conductor is surrounded with an infinite solenoid coil. For this problem, theoretical result is given in the book [11]. In this case only one segment region of the whole model can be the object of analysis due to axial symmetry, and modeled in FEM as depicted in Fig. 2. Here, hexahedral and penta element types are used. Boundary restraints are imposed upon two side faces such that $\mathbf{A}\times\mathbf{n}=0$ *and* $\varphi=0$ where $\mathbf{n}$ is the normal vector on the surface.

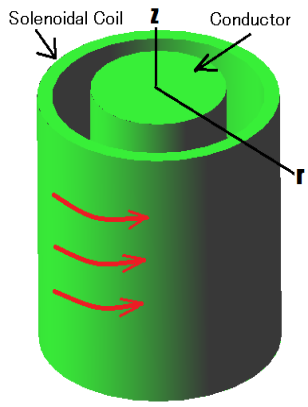

Fig. 1. Axisymmetric infinite solenoid problem.

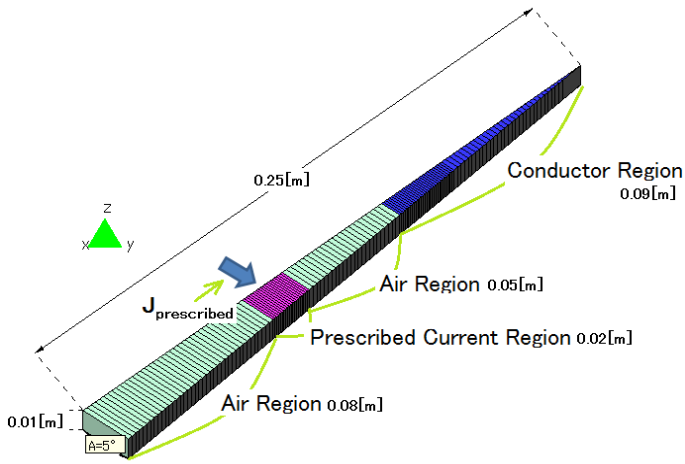

Fig. 2. FEM segment model of infinite solenoid problem

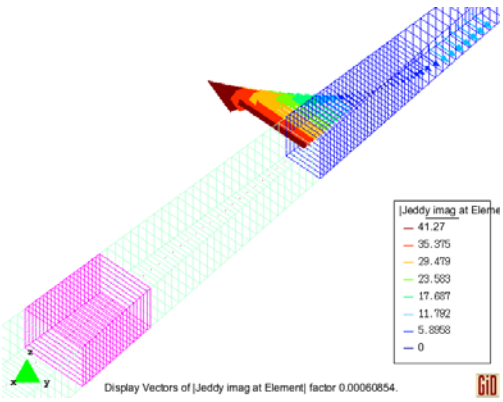

Fig. 3. Imaginary part of eddy current densities

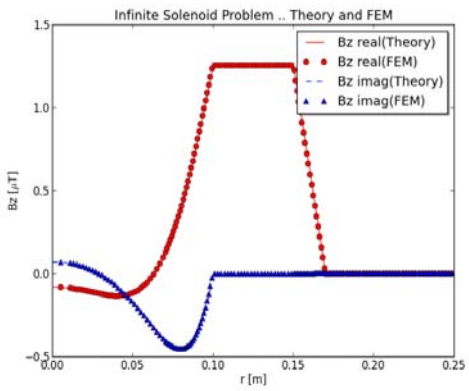

Fig. 4. Theory and FEM results of magnetic flux densities

The prescribed current density in the current region is 50.0 [A/m^2], the frequency is 60[Hz] and the electric conductivity is $7.7\times10^6\,[S/m]$. Vector plot of calculated eddy current densities of imaginary part is given in Fig. 3. A comparison of the theory and FEM result is given in Fig. 4 for magnetic flux densities against r coordinate. As in Fig. 4, the agreement of the theory and FEM result is very good, showing validity of the basic code.

B. A Wire Ring Connoted Versus A Wire Ring Disconnected

Although the infinite solenoid coil and conductor problem (*A.*) is a good example of code validation, there is still a room to discuss and notice. For rigorous axially symmetric problems, $-grad\varphi$ disappears because $\varphi(r,\theta_1,z)\equiv\varphi(r,\theta_2,z)$ $for\ \theta_1\neq\theta_2$. As the role of $-grad\varphi$ term is significant in Coulomb gauge, we must look forward to another example which clearly shows importance of $-grad\varphi$ in eddy current analysis.

If A.C. magnetic fields of uniform magnitude are exerted upon a metallic wire ring so that the direction of magnetic fields are perpendicular to the ring plane (see Fig. 5), circulating "eddy" current is induced as an introductory example of induction problem. And when the wire is cut at a point circulating current disappears. These two problems are modeled as the second example of validation.

In the calculation, the inner diameter of ring is 21[mm], the ring has rectangular cross section of 1[mm] x 1[mm]. For exerted magnetic field, frequency is 50[Hz] and amplitude is 10000[A/m]. The electric conductivity of ring wire is $60.0\times10^6\,[S/m]$.

The entire mesh is not shown in Fig. 5, the mesh of metallic ring shown in the figure are embedded in the entire space mesh. As the entire space mesh, elements are composed of hexahedral and penta types, number of nodes is 67,002, number of edges 204,097 and complex DOF is 204,401.

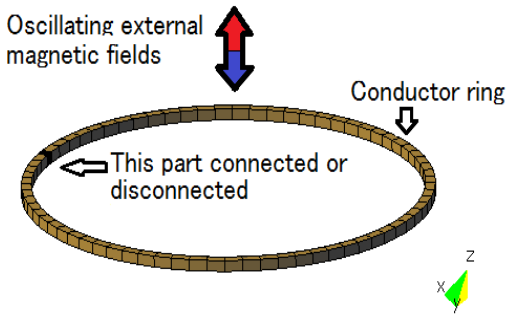

Fig. 5. Metallic wire ring example.

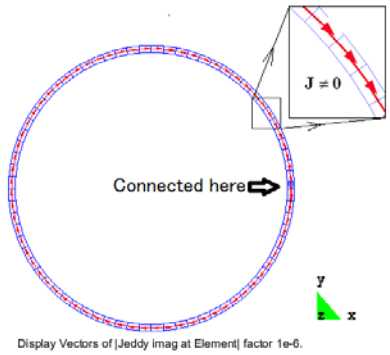

Fig. 6 Circulating "eddy" currents if connected

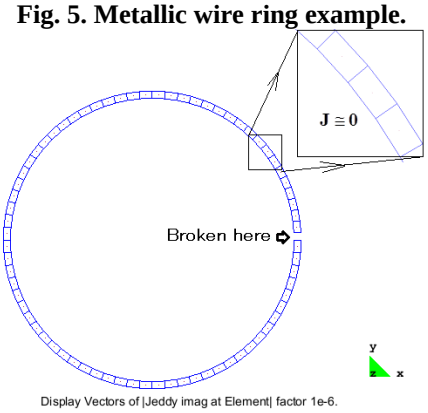

Fig. 7a. Eddy currents disappears if disconnected

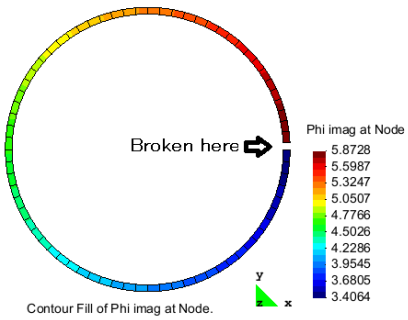

Fig. 7b. Imaginary part of φ if disconnected

Fig. 6, Fig. 7a and Fig. 7b are the FEM results. Fig. 6 and Fig. 7a are vector plots of eddy current densities for the connected ring (Fig. 6) and for the disconnected ring (Fig. 7a). The "eddy" current is circulating in the connected case, while it disappears in the disconnected case. And evident $-grad\varphi$ occurs as shown in Fig. 7b for the disconnected case. On the other hand, for the connected case, the $-grad\varphi$ term does not occur due to axial symmetry. Then the figure of contour plot of φ is trivial

and is not shown here.

For the connected case, a comparison of imaginary part of electric current density in a representative element is given in Table 1. It shows good agreement with the theory.

Table 1. Comparison of imaginary part of current density in an element.

	Theory	FEM result
J_{imag} $[A/m^2]$	-1.214E6	-1.211E6

For the disconnected case, $-grad\varphi$ and $-\dot{\mathbf{A}}$ almost cancels out with each other, resulting in disappearance of circulating eddy current. Such explicit cancellation is an obvious and significant feature of Coulomb gauge. In ECT problems, crack or slit is always assumed to exist and such cancellation mechanism should work in conductor regions especially in the vicinity of the crack or slit. From this sample and the consideration, we can conclude that the magnitude of $-grad\varphi$ term in Coulomb gauge can't be neglected in eddy current analysis of ECT problems.

C. An ECT Benchmark Problem of Single Pancake Type Coil

An experimental result of an ECT problem, in which single pancake type coil is placed above a flat metal plate involving a crack, is published in the literature [12] as a JSEM benchmark problem. Fig. 8 illustrates the conditions of the problem. Among several cases given in [12], the case of a rectangular slit residing in the metal surface is investigated here.

For the prescribed electric current, the frequency is 300[kHz], the amplitude is 8.0 [mA rms] and the number of coil turns is 140, the electric conductivity of the plate (Inconel 600) is $1.0\times10^6\ [S/m]$.

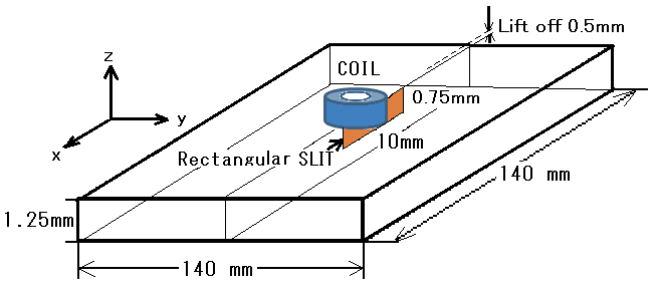

Fig. 8. An ECT problem of single pancake type coil

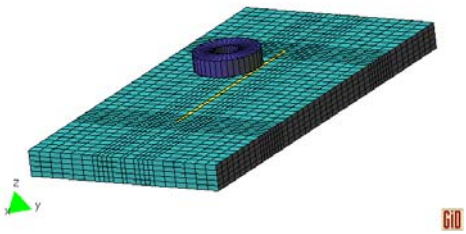

Fig. 9 FEM mesh and coil (essential part)

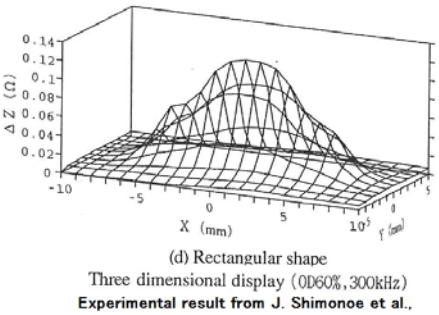

Fig. 10. Experimental impedance change given in [12]

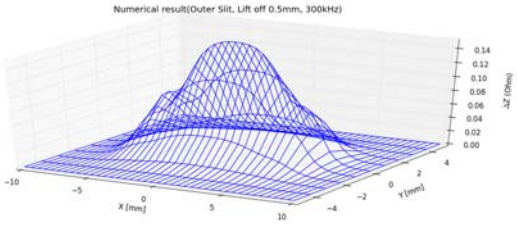

Fig. 11. Calculated impedance change

Fig. 9 illustrates the meshed model, where only the essential part of model is shown for briefness. For the entire mesh involving space mesh, the type of FEM elements is hexahedral only, number of nodes is 603,032, number of edges is 1,782,142 and DOF is 1,866,994. Fig. 10 is the experimental result referred to [12]. Fig. 11 is the FEM calculated result. Here only 1/4 area of xy plane is calculated and the others are extrapolated based on the symmetry rule. As seen in Fig. 11, the shape of impedance change profile is almost same to the experimental result of Fig. 10, although a small difference is observed in peak values between two figures that is $\Delta Z_{\exp} = 0.121$ while $\Delta Z_{ours} = 0.160$.

4. "TP01/A type/along crack" ECT problem – Numerical Experience

The Japan Society of Maintenology organizes round-robin tests and gathers non-destructive ECT signals freely available for anybody on the website [13]. Since we are not on the stage to make an inverse analysis and such a case of arbitrary shape crack made by tetrathionic acid is hard to model, it is difficult to show some useful results here. However, as a starting point of future work and for a numerical experience, a following analysis is possible assuming rectangular crack with some specific size. As an example, we chose "TP01/A type/along crack" ECT problem. Space, metal plate with slit and exciter coils are modeled as an FEM mesh and the conditions are;

Table 2. "TP01/A type/along crack" ECT problem

OS	Linux	RAM size	24Gbytes	Operation mode	Out of core	Frequency[kHz]	20,50,100
Nodes	657,018	Edges	1,937,691	DOF(Complex)	2,080,071	Element type	Hexahedral

The RAM size of 24G bytes was not enough to solve the problem with in-core mode. The illustration of the model is given in Fig. 12 and a sample output of eddy current profile is shown in Fig. 13. Electro-motive force with arbitrary scale is shown in Fig. 14.

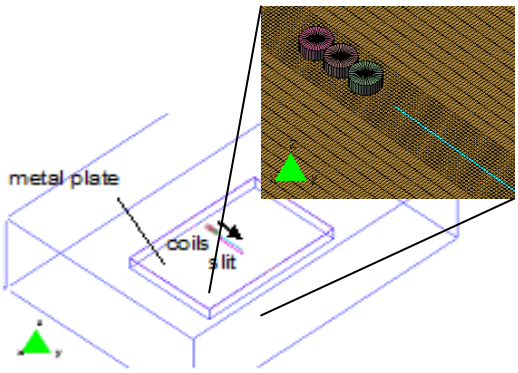

Fig. 12. A wireframe view of entire FEM Model

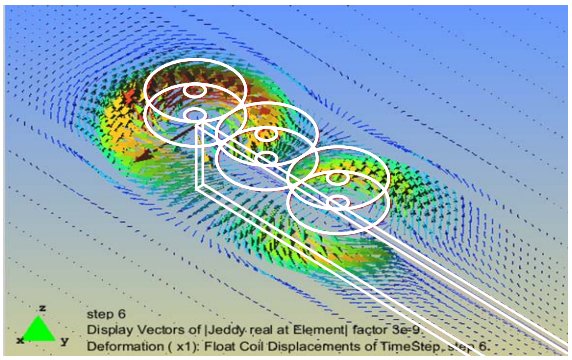

Fig. 13 A snap shot of eddy current density

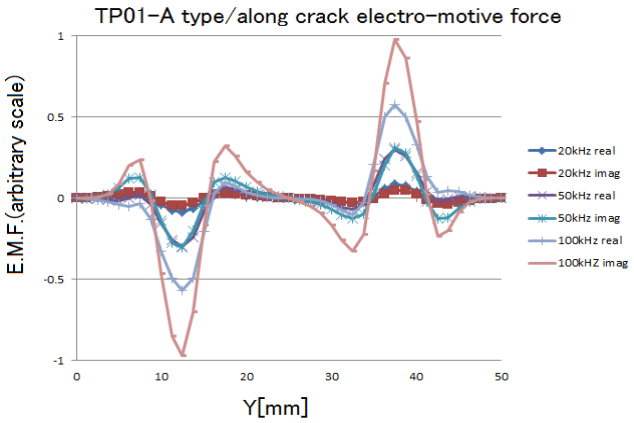

Fig. 14. Numerical result of electro-motive force in an arbitrary scale

The calculation is carried out for 20 coil positions as an example. Time consuming numerical factorization of sparse matrix is done only at the first step position. For other steps of 2nd to 20th, factorized matrix is reused repeatedly and calculation time is reduced as seen in Table 3. In Table 3, 65 minutes corresponds to numerical factorization while 38 minutes corresponds to Biot-Savart integration and solve phase of simultaneous equations. As seen in Table 3, time consuming numerical factorization is needed only at the first position of exciter coils.

The size of the problem in this section, is not extremely large, but it is near the end of the current author's hardware ability and is close to the realistic limit of our computation. If a bigger hardware is available for our work, our current practical limit, i.e., 2 million complex DOF, may be improved a

few factors. But we are guessing that improvement of several factors, i.e., 10 times or larger size, is not within the reality at this moment since CPU execution time of numerical factorization is proportional to DOF^3.

Table 3. Elapsed machine time for moving 20 positions of exciter/detector coils

Calculation phase	Elapsed time	# of positions	Total elapsed time
First position	103m (= 65m + 38m)	1	1h 43m
2nd~20th positions	38m (= 0m + 38m)	19	12h 02m
			13h 45m

5. Conclusion

In spite of many authors in the field of low frequency electromagnetic FEM tend to prefer iterative solvers for sparse simultaneous equations, the authors have paid attention to direct solver. It is emphasized that direct sparse solver is enough efficient in FEM-ECT analysis as long as the size is not very large (in short, problems having 2 million complex DOF are not extremely large within our current available hardwares). Especially for the case of moving exciter coils without ferromagnetic core, reuse of a numerically factorized matrix has been proved much useful and can be a practical means to reduce the computation time. This is an advantage of our approach compared with conventional works. While a disadvantage of direct solver is: that since CPU time of numerical factorization is proportional to DOF^3, long CPU time and large memory are required if problem size getting larger.

It is also emphasized that the term $-grad\varphi$ and the term $-\dot{\mathbf{A}}$ in Coulomb gauge, have almost close values and almost cancels with each other in the vicinity of crack and therefore neglect of term $-grad\varphi$ is not realistic in the framework of Coulomb gauge as discussed in the sample case of disconnected wire ring.

Acknowledgement

We would like to express our sincere thanks to Mr. Osamu Kounosu for his valuable advice.

References

[1] H. Fukutomi, T. Takagi, J. Tani, M. Hashimoto, J. Shimonoe and Y. Harada, “Numerical Evaluation of ECT Impedance Signal due to Minute Cracks”, IEEE Transactions on Magnetics, vol. 33, no.2, pp 2123-2126, 1997.
[2] T. Takagi, H. Huang, H. Fukutomi and J. Tani, “Numerical Evaluation of Correlation between Crack Size and Eddy Current Testing Signal by a Very Fast Simulator”, IEEE Transactoins on Magnetics, vol. 34, no.5, pp. 2581-2584, 1998.
[3] N. Yusa, Z. Chen, K. Miya, T. Uchimoto and T. Takagi, “Large-scale parallel computation for the reconstruction of natural stress corrosion cracks from eddy current testing signals”, NDT&E International 36 pp. 449-459, 2003.
[4] Y. Choua, L. Santandrea, Y. Le Bihan, and C. Marchand, Thin Crack Modeling in ECT With Combined Potential Formulations, IEEE Transactoins on Magnetics, vol. 43, no. 4, pp 1789-1792, 2007.
[5] H. Whitney, “Geometric Integration Theory”, Princten, NJ: Princeton University Press 1957.
[6] J. C. Nedelec, “Mixed finite elements in R^3”, Numer. Meth., vol. 35, 1980, 315-341.
[7] Jianming Jin, “The Finite Element Method in Electromagnetic”, JOHN WILEY & SONS, INC., 1993.
[8] As a review of “gauge fixing”, see the article of wikipedia: http://en.wikipedia.org/wiki/Gauge_fixing.
[9] Adventure project, “ADVETURE_Magnetic Non-Linear Magnetostatic / Time-Harmonic Eddy Current Analysis with HDDM Version 1.3 User’s Manual”, 2007; See http://adventure.sys.t.u-tokyo.ac.jp/
[10] P. R. Amestoy, I. S. Duff, J. Koster and J.-Y. L’Excellent, “A fully asynchronous multifrontal solver using distributed dynamic scheduling”, SIAM Journal of Matrix Analysis and Applications, Vol 23, No 1, pp 15-41 , 2001; See also http://graal.ens-lyon.fr/MUMPS/.
[11] For example, see Landau and Lifshitz, “Electrodynamics of Continuous Media”, Buttreworth Heinemann, problem 3. Of page 207.
[12] J. Shimone, K. Maeda and Y. Harada, Impedance Measurement of Unique Shape Cracks by Pancake Type Coil, JSAEM Studies in Applied Electromagnetics, 5, pp.12-17 ,1996.
[13] http://jsm.or.jp/jsm/at/scc/index_eng.htm